JOURNAL OF MATERIALS SCIENCE 26 (1991) 3544–3552

Microstructure and micromechanics of the interface in carbon fibre reinforced Pyrex glass

S. M. BLEAY, V. D. SCOTT
School of Materials Science, University of Bath, Claverton Down, Bath BA2 7AY, UK

Detailed microstructural studies have been carried out on composites consisting of Pyrex glass reinforced with carbon fibres. Analysis of the fibre–matrix interface showed that some reaction had taken place during fabrication of the composite and that a carbide or oxycarbide layer had formed between the glass and the carbon fibre. The measured interlaminar shear strength of the composite indicated that the layer was not a source of weakness and appeared to be well bonded to the matrix. Substantial fibre pull-out had occurred, however, to expose clean fibre surfaces and smooth sockets. These observations led to the conclusion that the interfacial shear process was confined substantially to the outer layers of the carbon fibre. Confirmatory evidence for the low interfacial friction stress was available from micro-indentation tests which showed fibre displacement relative to the matrix at loads of less than ~10 kPa. Heat treatment of the composite at 500 °C in air caused preferential oxidation of the carbon fibre. Where fibres met the specimen surface, oxidation had proceeded down the fibre to produce a smoothly tapering shape. The rate of oxidation was estimated to be 3 $\mu m\,h^{-1}$ parallel to the fibre axis, but much less than this in a direction perpendicular to the fibre, 0.5 $\mu m\,h^{-1}$, due to the relatively slow diffusion rate of oxygen through glass.

1. Introduction

The concept of glass matrix composites has been considered since the 1960s but at that time fibre technology was not sufficiently advanced to produce satisfactory composites, the fibres available being generally monofilaments several hundreds of micrometres in diameter which simply acted as stress concentrators when incorporated into the glass.

With the development, however, of a range of relatively cheap, small-diameter ceramic fibres, interest in these materials was revived. In the early 1970s, a comprehensive study was carried out by Phillips and co-workers [1–4] into the use of carbon fibres, both continuous and discontinuous, for reinforcing glass, glass–ceramic and ceramic matrices. Their results on Pyrex glass reinforced with short (~ 200 μm) carbon fibres showed increases in the work of fracture and thermal shock resistance, although the use of randomly oriented fibres actually lowered the strength below that of the parent glass [1]. When reinforced with continuous fibres of carbon, strengths were obtained which approached that predicted by the Rule of Mixtures, the high work of fracture being attributed to fibre pull-out during the test [2, 4]. The strength of the composite was maintained up to temperatures of ~ 500 °C in an inert atmosphere but performance in air was limited by the oxidation of the carbon fibre. Recent studies by Prewo and Batt [5] showed that oxidative attack occurred much more rapidly parallel to the fibres, leading to the conclusion that loss of strength would depend upon the size of a component and its fibre configuration. Work is still continuing on this system, in particular the modification and improvement of the fibre–matrix interface using additives to the glass [6], and the characterization of failure modes [7]. Carbon is not the only reinforcing fibre that has been used in Pyrex glass and investigations have been carried out [8–10] on Nicalon [11], a silicon-carbide based fibre developed in the 1970s and claimed to be thermally stable to 1000 °C.

In the present paper new results on Pyrex reinforced with carbon fibres are reported which include detailed microstructural studies with particular reference to the fibre–matrix bond as a function of thermal treatment in air. The results are compared and contrasted with earlier studies on Pyrex glass reinforced with Nicalon fibres [12].

2. Experimental procedure

2.1. Materials

Composite material consisting of Pyrex glass reinforced with Hercules Magnamite HM carbon fibres was provided in the form of 10 cm × 10 cm plate. It was manufactured at AEA Harwell by hot pressing [1] at a temperature of 1100–1200 °C and a pressure of ~ 4 MPa.

2.2. Microstructural examination

Samples of composite were ground into powder and X-ray diffraction (XRD) carried out in a Philips PW1820 diffractometer for analysis of crystalline phases.

0022–2461/91 $03.00 + .12

Sections 10 mm thick were cut from the composite plate with a resin-bonded diamond saw rotating at a low speed to minimize cutting damage. The sections were mounted in a cold-curing epoxy resin, degassed for 5 min, and ground on a water-lubricated diamond wheel using a force of 22 N per sample to produce a planar surface. The majority of the grinding damage was removed by polishing with 6 μm diamond slurry for 10 min on a Buehler Metlap 4 wheel contra-rotating at 25 r.p.m. This was followed by 10 min on a Buehler Metlap 2 wheel at 120 r.p.m. using 6 μm diamond slurry, 10 min on a Buehler Metlap 1 wheel at 120 r.p.m. using 1 μm diamond slurry and colloidal silica, and a one-minute water wash.

Polished sections were examined in a Zeiss ICM 405 optical microscope fitted with Nomarski interference. Subsequent analyses were performed in a scanning electron microscope (SEM), a Jeol 35C microscope fitted with backscattered electron imaging (BEI) and a Link AN10000 energy-dispersive X-ray spectrometer (EDS) for compositional analysis. SEM was also performed on composite sections etched in HF for 2.5 h, on fracture surfaces of unidirectional and cross-ply plates, and on specimens broken parallel to the fibre direction after heating at 500 °C in air for 0, 60 and 160 h. All samples for SEM study were coated with gold prior to examination.

Transmission electron microscopy (TEM) was performed on thin foil specimens prepared from as-received composite and on material which had been heated in air at 500 °C for 24 h. The thin sections were prepared as follows. Discs of 3 mm diameter were cut from bulk material with a diamond-tipped coring drill and mechanically ground to a thickness of ~ 300 μm on 400 grit SiC paper. They were then dimpled on both sides on a VCR Model D500 so as to leave a central specimen thickness of ~ 20 μm. Final thinning was carried out by argon-ion bombardment in a Gatan Duomill at 5 kV with an incidence angle of 15° until sample perforation, then with an incidence angle of 7° to extend the thinned area. TEM studies were performed in a Jeol 2000FX microscope fitted with a Link AN10000 EDS system with high-angle thin-window detector. Bright-field, selected-area diffraction (SAD), micro-diffraction and EDS modes of analysis were employed.

2.3. Interface friction measurements

Comparative values of fibre–matrix interfacial friction stress for the composites were obtained by carrying out micro-indentation tests [13] on polished transverse sections. A load of 0.25 N was applied to the centres of 20 different fibres using a Leco M-400 hardness tester such that an indentation was produced which extended some distance into the glass matrix. The friction stresses were obtained from the equation

$$\tau = F^2/4\pi^2 u R^3 E_f$$

where R is fibre radius, E_f is fibre modulus (380 GPa for carbon) and F is the force applied to the fibre. The term u represents fibre displacement at maximum load and can be calculated from measurements of indentations in both fibre and matrix.

3. Results

3.1. X-ray diffraction studies

The XRD trace from the carbon–Pyrex composite, Fig. 1, shows peaks indexed as graphite. No other crystalline phase was present in sufficient amounts to be detectable by this technique.

3.2. Optical microscopy

A transverse section of a composite containing unidirectionally aligned carbon fibres is illustrated in Fig. 2a. The fibre size is 8 ± 1 μm and the distribution is generally uniform, although the form of the original fibre tows remains clearly evident. The fibre volume fraction was estimated as 0.36 ± 0.04 and some porosity was visible, amounting to no more than 1 vol %. A longitudinal section of the same plate (Fig. 2b) shows features in the matrix ~ 20 μm in size (marked A).

3.3. Scanning electron microscopy

Whilst backscattered electron imaging in the SEM (Fig. 3) shows the fibres as being darker than the surrounding matrix due to their lower mean atomic number, the matrix features (A in Fig. 2b) do not apparently differ sufficiently in composition from the surrounding matrix to produce contrast. Their presence was, however, confirmed after heavily etching the composite in HF (Fig. 4a). Preferential etching is seen to have taken place around this type of particle, which EDS (Fig. 4b) shows to consist primarily of carbon; the gold X-ray peak originates from the coating on the specimen. Another phase was located in the matrix (Fig. 4c) and this was found to contain silicon, oxygen and a trace of aluminium (Fig. 4d), a composition indicative of cristobalite [12] which is a polytype of silica.

3.4. Fractography

SEM examination of the tensile fracture surfaces of the unidirectional carbon–Pyrex sample (Fig. 5) showed that it had failed in a predominantly brittle fashion; furthermore, the fracture path did not appear to have occurred perpendicularly to the test direction but at an angle of $\sim 30°$ to the longitudinal axis.

The fracture mode of the cross-ply plate was different and showed evidence of fibre pull-out in the 0° plies (area I in Fig. 6a) and fragmentation of the matrix around fibres in the 90° plies (area II in Fig. 6a). A higher-magnification picture of area I (Fig. 6b) shows a maximum pull-out length of ~ 60 μm with clean fibre surfaces and smooth "sockets"; no evidence of matrix adhering to the carbon fibre was found.

Examination of specimens heated in air at 500 °C and broken parallel to the fibres shows the effects of progressive fibre oxidation. Fig. 7a, taken from the edge of a specimen of as-received material, shows

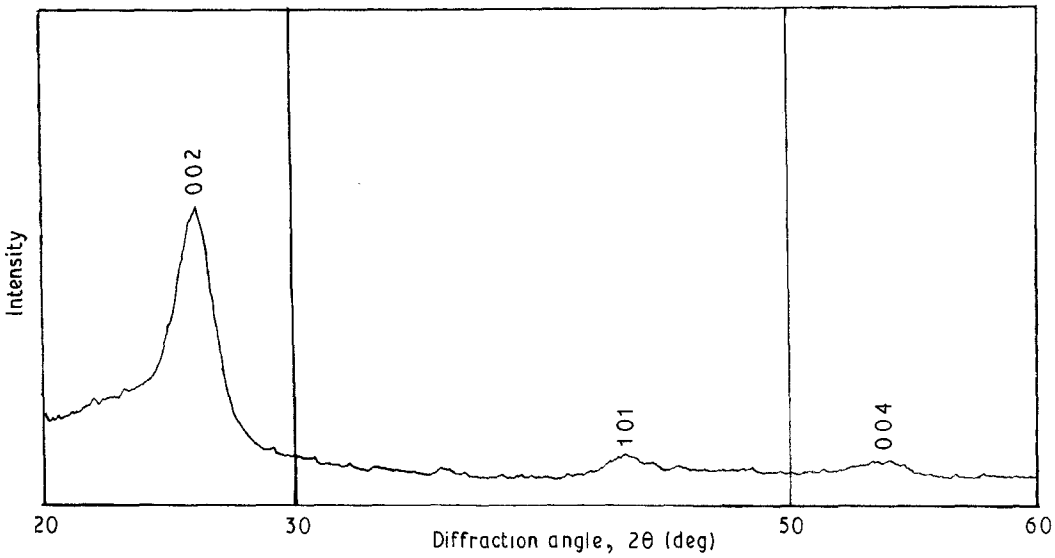

Figure 1 X-ray diffraction from powdered carbon–Pyrex composite, showing graphite diffraction peaks.

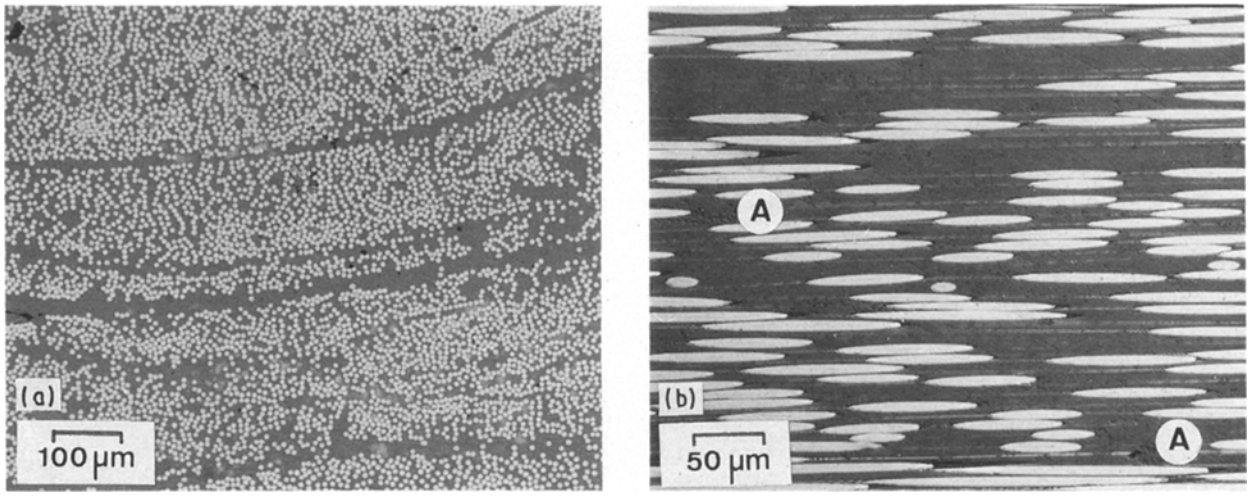

Figure 2 Polished sections of composite, optical microscopy: (a) transverse section, showing fibre distribution; (b) longitudinal section, showing second phase (A) in matrix.

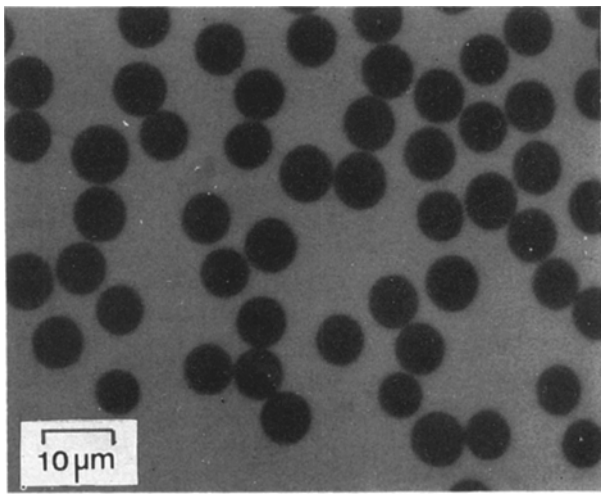

Figure 3 Polished section of composite, SEM backscattered image.

clean fibre surfaces after separation from the glass matrix.

After ageing for 60 h (Fig. 7b), fibres at the edge of the specimen have begun to oxidize, giving them a tapered appearance as their carbon is converted to CO_2. Fibre degradation has also taken place where fibres run close to the surface of the specimen (Fig. 7c), oxidation proceeding inwards from the surface marked A with fibres in the left side of the picture showing clear evidence of attack along the whole fibre length. Fig. 7d, taken from the edge of a specimen aged for 160 h, shows that fibre oxidation has proceeded to such an extent that there is an outer layer of the composite, $\sim 500\ \mu m$ thick, where the fibres have oxidized away to leave a "honeycomb" of matrix. The remaining fibres are needle-like (A), tapering towards the surface exposed to the atmosphere as in Fig. 7b. Fibre damage in the form of pits caused by oxidation of these fibres close to the surface is illustrated in Fig. 7e. Estimates of oxidation rate made from the above micrographs gave $0.5\ \mu m\ h^{-1}$ perpendicular to the fibres and $3\ \mu m\ h^{-1}$ along the fibres.

3.5. Thin foil studies

Thin foil studies in the TEM of the glass matrix showed it to be generally homogeneous. Some features

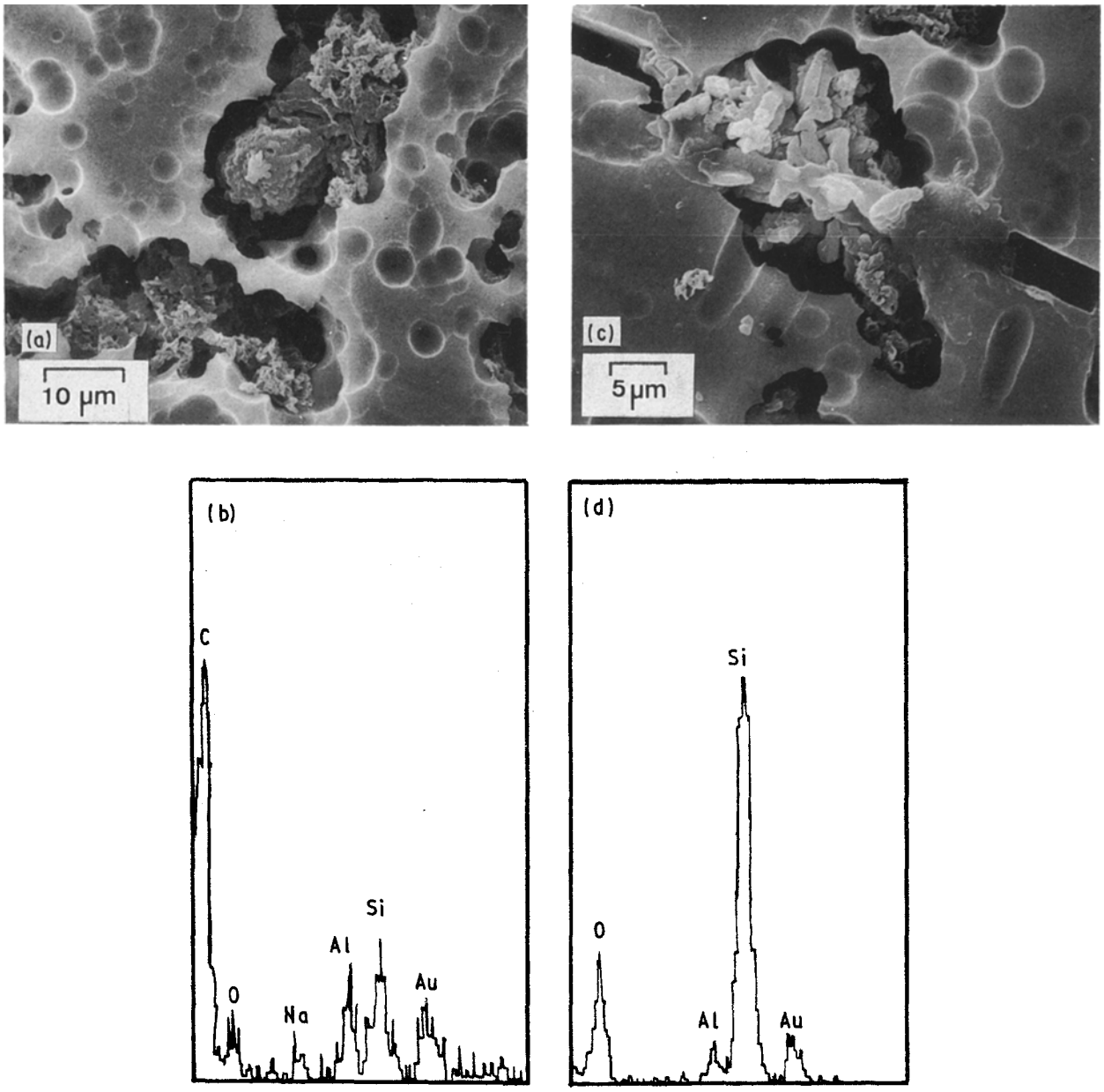

Figure 4 Composite after etching in HF: (a) second phase in matrix, (b) EDS of second phase, (c) cristobalite in matrix, (d) EDS of cristobalite particle.

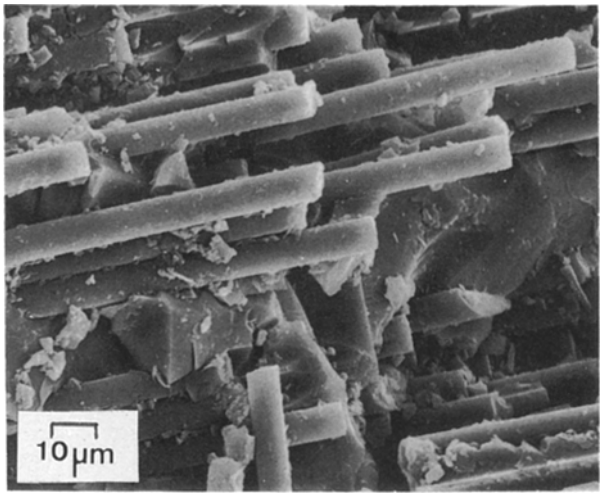

Figure 5 Unidirectional composite, fracture surface, SEM.

possibly related to the second-phase particles seen in the SEM were present (Fig. 8) which appeared to contain cavities. EDS from these regions did not, however, show the presence of a high carbon level but a composition close to that of the surrounding Pyrex matrix. These regions were shown to be amorphous by selected-area electron diffraction.

A fibre–matrix interface is illustrated in Fig. 9a. The carbon fibre (region I) shows a textured structure which selected-area electron diffraction (Fig. 9b) indicates is associated with basal planes lying parallel to the fibre axis with a misorientation about it of $\pm$ 15°. There appears to be no sharp transition between fibre and matrix, although a more electron-transparent zone $\sim$ 100 nm thick is visible between them. EDS data from the fibre (region I) shows that it has a trace of sodium (Fig. 9c) which is difficult to explain. The

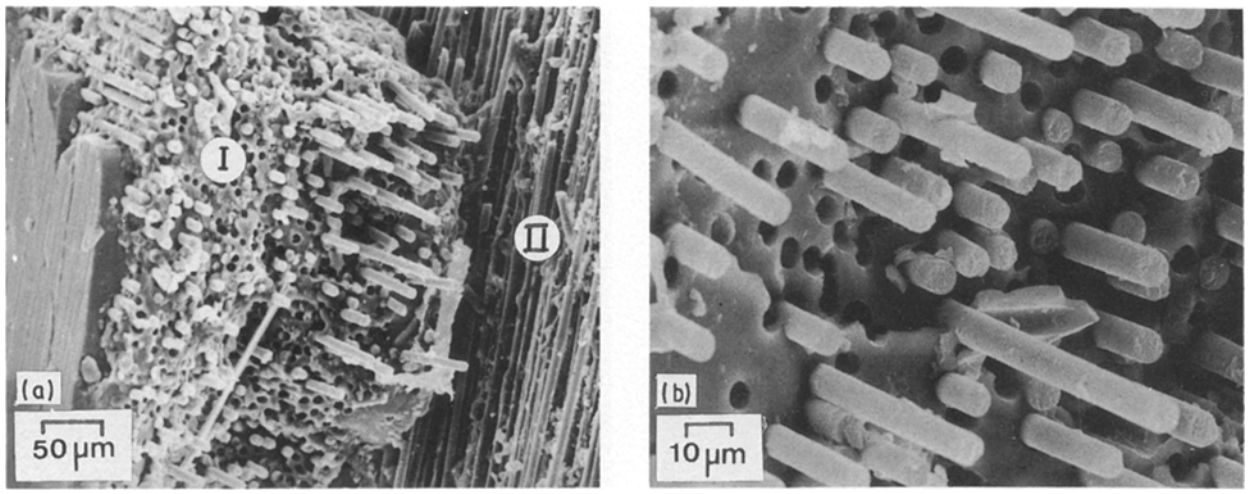

Figure 6 Cross-ply composite, fracture surface, SEM: (a) low magnification, (b) high magnification, showing clean fibre pull-out.

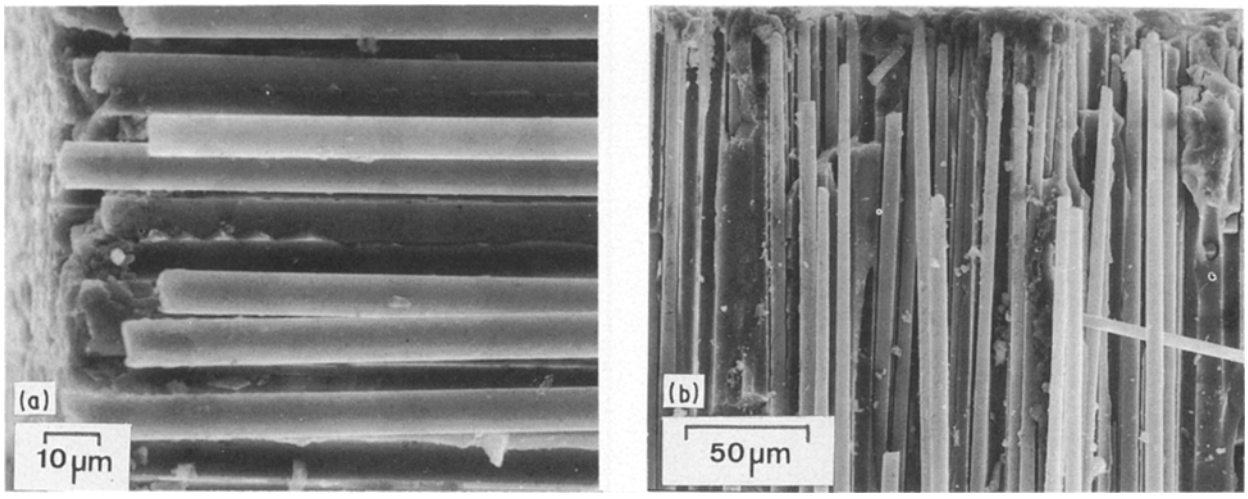

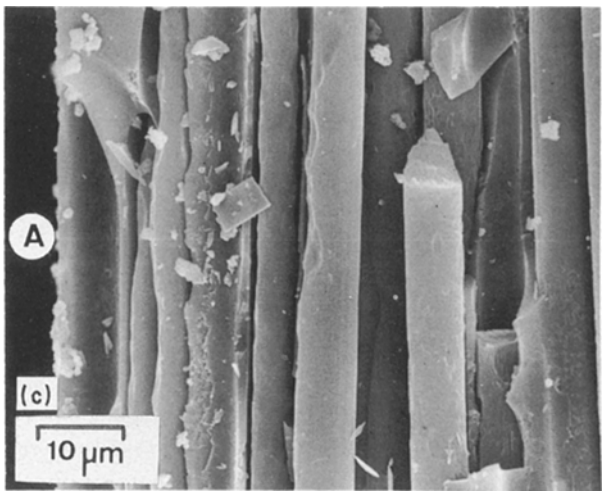

Figure 7 Oxidized carbon–Pyrex composites, SEM: (a) as-received material; (b) after ageing for 60 h, surface parallel to fibres; (c) after ageing for 60 h, surface perpendicular to fibres; (d) after ageing for 160 h, surface parallel to fibres; (e) after ageing for 160 h, fibres close to surface.

interfacial zone (region II) contained a significant amount of carbon together with oxygen, silicon and sodium (Fig. 9d), whilst the adjacent matrix (region III) shows oxygen, sodium, aluminium and silicon peaks (Fig. 9e) consistent with the Pyrex glass composition. Some areas of matrix close to the fibres were found to be denuded in sodium by $\sim 50\%$.

TEM of a specimen taken from a region of oxidized composite showed formation of voids at the fibre edge (Fig. 10a). Void formation was also seen in the matrix close to the fibre (Fig. 10b). The two areas shown in Fig. 10a and b were initially in contact, but easily separated when the electron beam was focused on them. This observation would suggest that the void formation caused by oxidation substantially weakens the fibre–matrix bond and allows easy debonding.

3.6. Interface friction measurements

In the indentation test on as-received composite the fibres slid easily, even under minimal loads. The ease of fibre sliding is illustrated in Fig. 11a, which shows an indented fibre and an adjacent impression in the matrix after applying a load of 0.25 N. It was not possible to calculate a value of interfacial friction stress, due to the fact that the indenter did not leave an impression on the fibre, but clearly it was low. This assumption is consistent with Fig. 11b, which shows deflection of a crack around more than twenty fibres

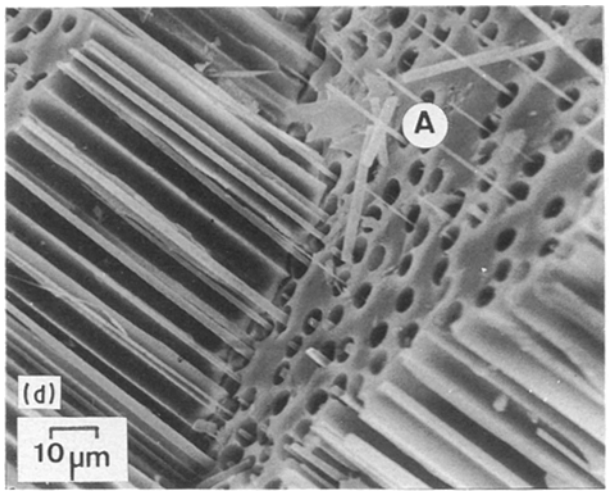

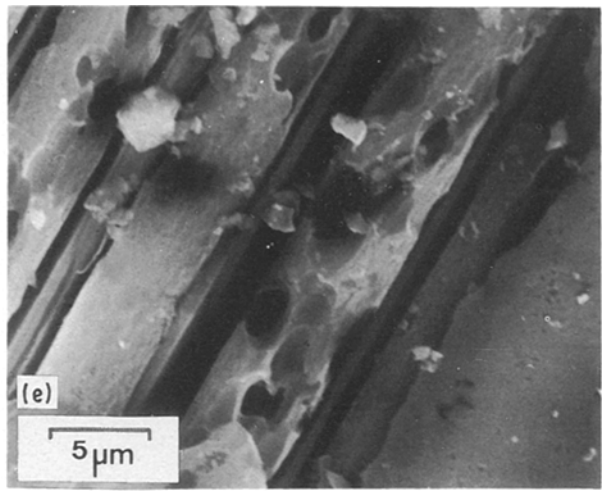

Figure 7 continued

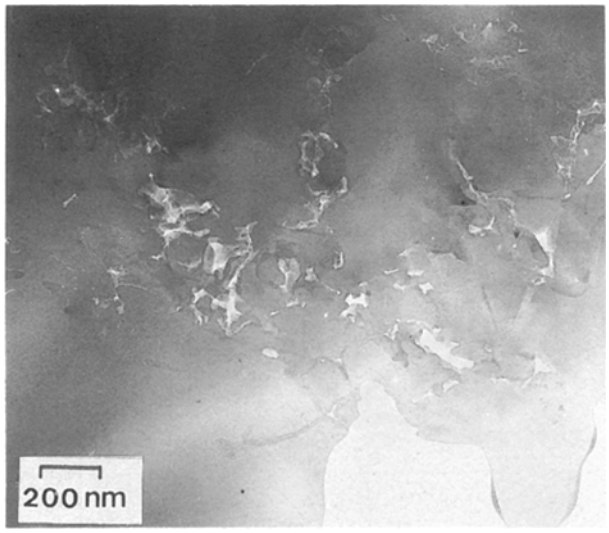

Figure 8 Second phase in matrix, TEM.

coupled with separation at the fibre–matrix interface. Calculation of an upper-bound limit assuming minimal indenter contact with the fibre gives ~ 10 kPa, a value several orders of magnitude lower than observed for other composite systems.

4. Discussion

4.1. The composite

EDS measurements in both TEM and SEM have shown the carbon fibres to contain traces of sodium impurity of unknown origin. Crystallographic analysis has shown the fibres to be graphitic, with a preferred alignment of basal planes of the graphite lattice parallel ($\pm$ 15°) to the fibre axis.

The matrix of the composite was found to contain discrete particles of irregular shape (Fig. 4a) which EDS showed to consist substantially of carbon. Thin-foil studies in the TEM revealed some porosity associated with these particles. The cause of their formation is uncertain, but a likely possibility is that they are binder residues resulting from incomplete burn-off prior to the hot-pressing procedure, i.e., as the resin binder oxidizes during fabrication, cavities are formed together with carbon deposits in adjacent regions.

Less frequently, a second type of matrix constituent was discovered which consisted primarily of silicon and oxygen. It is considered that the phase is cristobalite, as reported previously in our studies on hot-pressed Pyrex glass composites reinforced with Nicalon fibres [12]. The failure of XRD to reveal any crystalline phase in the composite other than graphite indicates that the cristobalite amounts to no more than 5% by volume, the limit of detection for this technique. It should be noted that the higher processing temperature (1100–1200 °C) used in manufacturing the carbon–Pyrex composites has resulted in a much reduced proportion of cristobalite.

4.2. The fibre–matrix interface

The microstructure of the interface between carbon fibre and Pyrex glass matrix was seen in the transmission electron microscope as a ~ 100 nm wide zone of more electron-transparent material than either fibre or matrix. The absence of a sharp demarcation between fibre and matrix suggests some reaction has taken place during the hot-pressing cycle. Indeed, Tredway *et al.* [6] have referred to thermodynamic calculations which would indicate that carbide or oxycarbide reaction products may form at the interface. This would accord with present results which showed the presence of the elements carbon, oxygen and silicon, together with a significant amount of sodium, more than normally found in the Pyrex glass. Our evidence then leads to the conclusion that there is a thin layer of sodium-enriched silicon oxycarbide adjacent to the carbon. The higher electron transparency of the layer must be due to a greater degree of thinning in the ion-beam apparatus, rather than the possibility that it has a lower atomic number than the adjacent material.

With regard to the mechanical properties of the interface, available data [7] from bend tests carried out on unidirectionally aligned material with the bending axis perpendicular to fibres gave interlaminar shear strength values of ~ 39 MPa, indicative of a

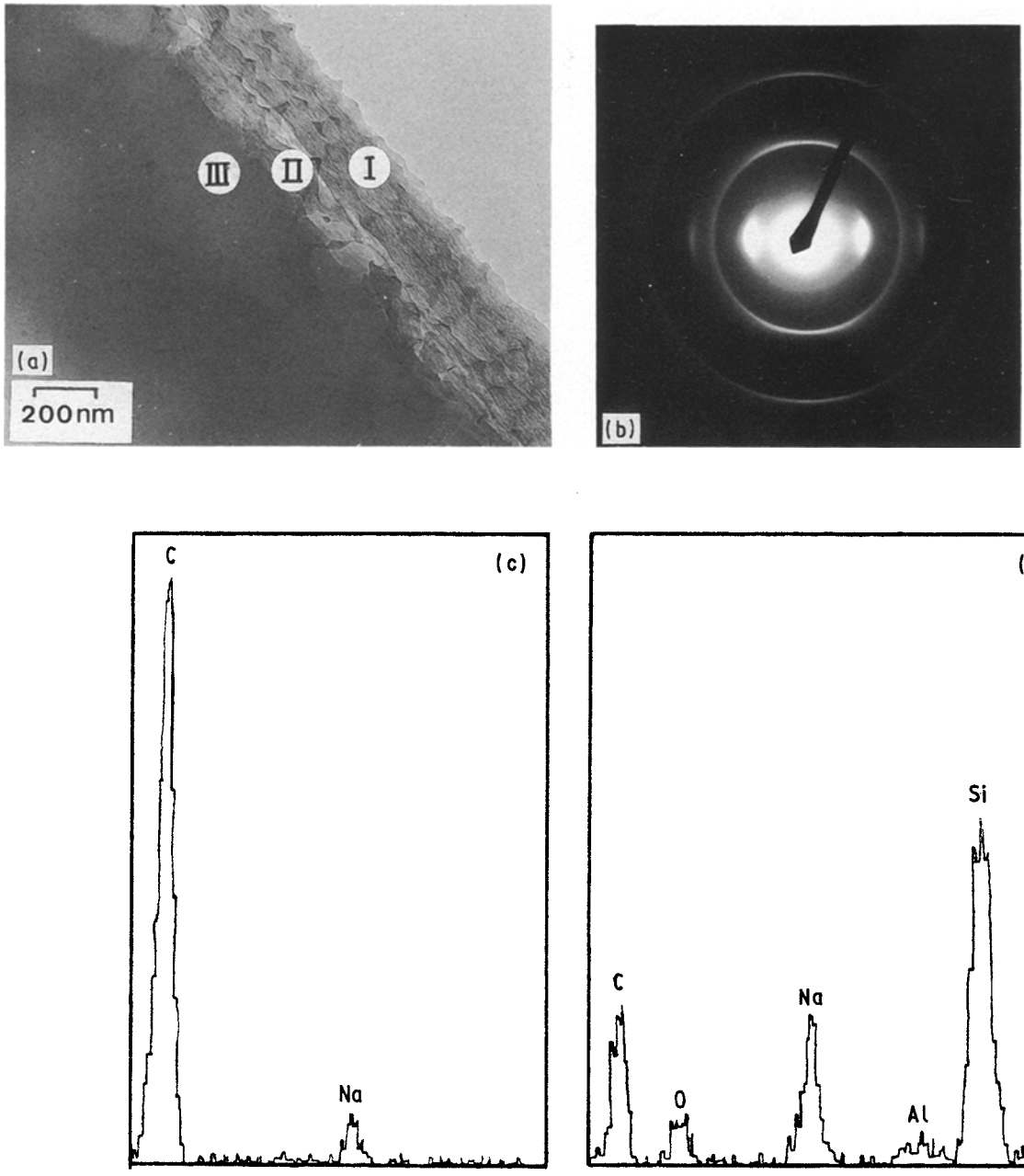

Figure 9 Fibre–matrix interface, TEM: (a) TEM showing fibre (I), interface (II) and matrix (III); (b) SAD from region I; (c) EDS from region I; (d) EDS from region II; (e) EDS from region III.

reasonably good fibre–matrix bond. Tredway *et al.* [6] have also noted reasonably good fibre–matrix bonds in carbon fibre–borosilicate glass composites and, using an instrumented indentation test, recorded debonding stresses ranging from 16 to 38 MPa depending upon the interface chemistry.

Once interface debonding has occurred during a test, substantial fibre pull-out can occur, as evidenced in the 0° plies of the cross-ply plate where fractography (area 1 in Fig. 6a) shows exposed fibres with clean surfaces and smooth "sockets". The lack of any matrix material adhering to the carbon fibre suggests that the shear interface is confined to the outer layers of the carbon fibre and that the oxycarbide reaction product has remained substantially in contact with the Pyrex glass. Such a shearing action would be promoted by (a) the observed alignment of graphite basal

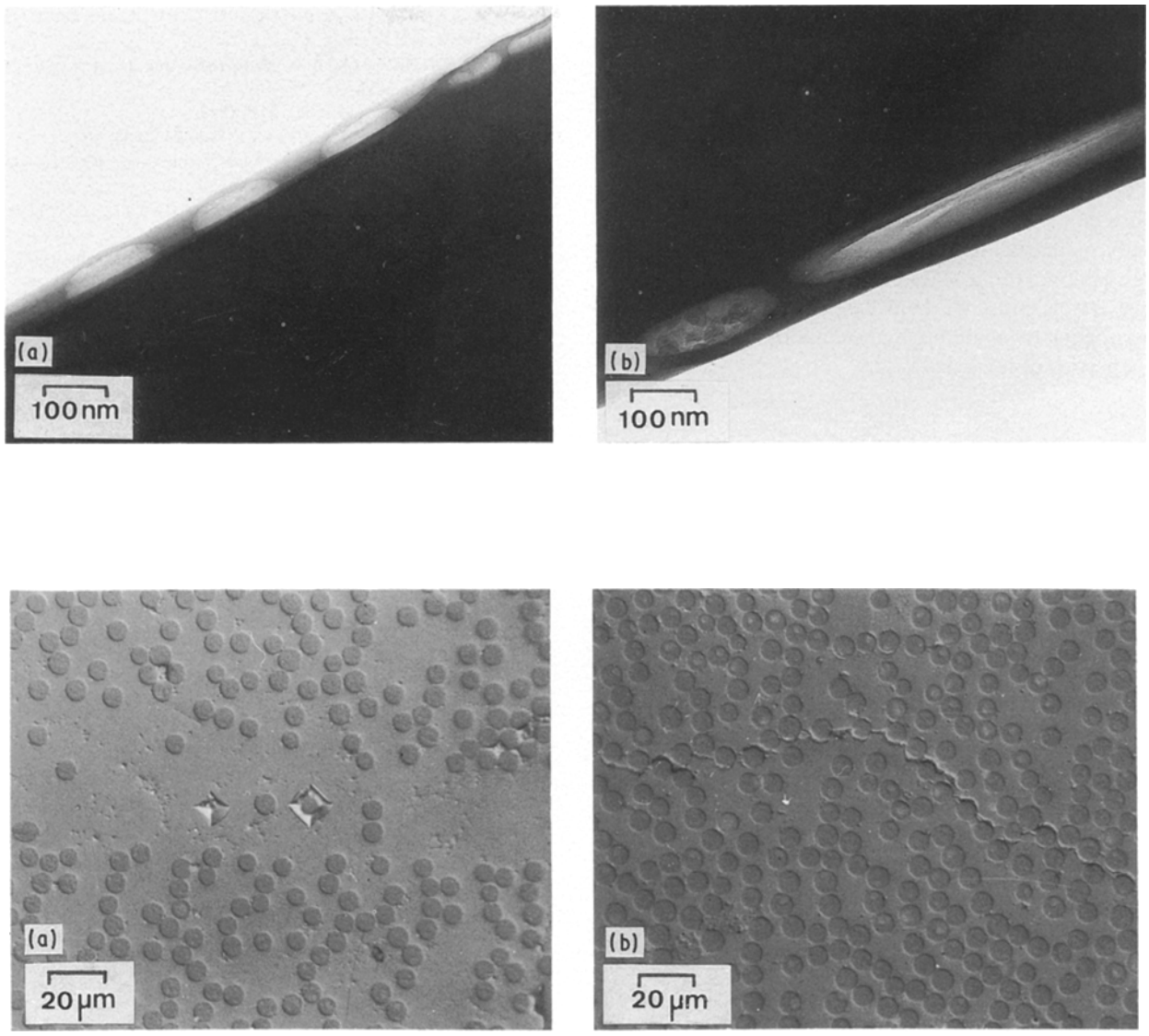

Figure 11 Polished sections of composite, optical microscopy: (a) micro-indentation on fibre and matrix, (b) crack deflection around fibres.

planes parallel to the surface which then act as solid lubricant, and (b) the greater degree of thermal contraction of the carbon (transverse coefficient of thermal expansion $= 8 \times 10^{-6}\ K^{-1}$) which results in the development of radial tensile stresses at the carbon interface. It should be noted that we consider the oxycarbide layer as being part of the glass component, since it has a similar thermal expansion coefficient and appears to be well bonded to the glass. Strong evidence for the existence of a low interfacial friction stress is available from our results from micro-indentation experiments. Upon first applying the indenter, the load ($\sim$ 1 GPa) is more than adequate to debond the fibre from the matrix and thereafter only a very low stress is required to overcome interfacial friction. The crack-deflecting capability of this type of interface is evidenced in Fig. 11b, where a crack has passed around more than 20 fibres.

It is of interest to compare the microstructure and micromechanics of the interface in this system with Nicalon-reinforced Pyrex glass. The bond strengths of the respective fibre–matrix interfaces were comparable, but the interfacial friction stress was much higher in the latter material. There were, however, differences between the two microstructures in that the carbon layer at the Nicalon–Pyrex interface [12] was very much thinner ($\sim$ 10 nm) and was not oriented with basal planes parallel to the surface, both features being expected to result in the observed reduction in lubricating action.

4.3. The effect of heating the composite in air

Studies of composites broken open after heating in air at 500 °C showed preferential oxidation of the fibres. Where fibres met the specimen surface, oxidation had proceeded down the fibre to produce a smoothly tapered shape indicative of a uniform rate of oxidation around the fibre. With increase in oxidation time, the ends of fibres had been totally decomposed to leave a Pyrex matrix with a network of holes. Estimates of the oxidation rate gave 3 $\mu m\ h^{-1}$ parallel to the fibre axis. In the direction perpendicular to the fibres the oxidation rate was very much lower, 0.5 $\mu m\ h^{-1}$, due to the relatively slow diffusion of oxygen through the glass. The attack on the fibre surface was then much more localized to give a pitted appearance, as evidenced by

SEM examination of the fibre surface and the voids revealed in TEM studies of thin sections.

These observations are in general accord with those of Prewo and Batt [6] who carried out similar oxidation studies on a carbon–Pyrex system. They reported preferential oxidation parallel to the fibres and less severe attack on specimen edges perpendicular to the fibre but, whilst showing an increase in oxidation rate with increased temperature, did not quote specific values concerning reaction rates. Clearly, such oxidative effects must be considered when designing experiments to evaluate high-temperature mechanical properties of these materials.

Acknowledgements

The authors would like to thank Rolls Royce plc for financial support, Mr R. J. Lee of AEA Harwell for supplying the composite material, the Rev. B. Chapman for assistance with X-ray diffraction studies and the SERC for support of electron optics facilities.

References

1. R. A. J. SAMBELL, D. H. BOWEN and D. C. PHILLIPS, *J. Mater. Sci.* **7** (172) 663.
2. R. A. J. SAMBELL, A. BRIGGS, D. C. PHILLIPS and D. H. BOWEN, *ibid.* **7** (1972) 676.
3. D. C. PHILLIPS, R. A. J. SAMBELL and D. H. BOWEN, *ibid.* **7** (1972) 1454.
4. D. C. PHILLIPS, *ibid.* **9** (1974) 1847.
5. K. M. PREWO and J. A. BATT, *ibid.* **23** (1988) 523.
6. W. K. TREDWAY, K. M. PREWO and C. G. PANTANO, *Carbon* **27** (1989) 717.
7. F. A. HABIB, R. G. COOKE and B. HARRIS, *Br. Ceram. Trans. J.* **89** (1990) 115.
8. B. A. FORD, R. G. COOKE and S. NEWSAM, *Br. Ceram. Proc.* **39** (1987) 229.
9. A. BRIGGS and R. W. DAVIDGE, *Mater. Sci. Engng* **A109** (1989) 363.
10. K. M. PREWO and J. J. BRENNAN, *J. Mater. Sci.* **17** (1982) 1201.
11. S. YAJIMA, K. OKAMURA, J. HAYASHI and M. OMORI, *J. Amer. Ceram. Soc.* **59** (1976) 324.
12. S. M. BLEAY and V. D. SCOTT, *J. Mater. Sci.* **26** (1991) 2229.
13. D. B. MARSHALL and A. G. EVANS, *J. Amer. Ceram. Soc.* **68** (1986) 225.

Received 10 August
and accepted 4 September 1990